Cancer Imaging

RESEARCH

Open Access

Quantitative parameters of dual-layer spectral CT for differentiating metastatic and non-metastatic lymph nodes in colorectal cancer

Liyan Tang[1,2], Guoqing Liu[1], Xia Lv[1], Weicui Chen[1*] and Xian Liu[1*]

Abstract

Background To investigate the value of quantitative parameters obtained from dual layer spectrum CT (DLSCT) in distinguishing metastatic and non-metastatic lymph nodes in colorectal cancer (CRC).

Methods This retrospective study enrolled 211 LNs from 66 CRC patients, including 78 metastatic LNs and 133 non-metastatic LNs. The morphological characteristics and quantitative DLSCT parameters of each identified lymph node were evaluated and compared. Univariate and multivariable logistic regression analyses were used to identify the independent factors for predicting LN metastasis. Receiver operating characteristic curve (ROC) and decision curve analysis (DCA) were employed to evaluate the diagnostic performance and clinical usefulness of the models.

Results All morphological features differed between metastatic and non-metastatic LNs. Metastatic LNs showed significantly lower iodine concentration (IC) and normalized iodine concentration (NIC) in the arterial phase, while exhibiting higher effective atomic number (Zeff), normalized effective atomic number (nZeff) in the venous phase, and slope of the spectral Hounsfield unit curve (λHu) values in both phases. A positive correlation was found between λHu values of LNs and tumors in both the arterial and venous phases within the LN metastasis group. For differentiating metastatic and non-metastatic LNs, combined morphological features yielded an AUC of 0.695, with 66.7% sensitivity and 68.4% specificity, while a multivariate model incorporating DLSCT parameters improved this to 0.901, with 82.1% sensitivity and 87.2% specificity. The DeLong test and decision curve analysis (DCA) showed that quantitative multiparameter model offered better predictive performance and benefits for LN metastasis than the morphological features.

Conclusion Quantitative parameters from DLSCT provide significant value in distinguishing lymph node metastasis in colorectal cancer.

Keywords Dual-layer spectral detector CT, Colorectal cancer, Lymph node metastasis

*Correspondence:
Weicui Chen
weicuichen@126.com
Xian Liu
liuxian74@hotmail.com
[1]Department of Radiology, The Second Affiliated Hospital of Guangzhou University of Chinese Medicine, Guangzhou 510120, China
[2]The Second Clinical College of Guangzhou University of Chinese Medicine, Guangzhou 510006, China

Background

According to Global Cancer Statistics 2024, colorectal cancer (CRC) is the third most common cancer globally, representing about 10% of all cancer cases and being second only to lung cancer in terms of cancer-related mortality [1]. Lymph node metastasis (LNM) is a significant pathological characteristic of CRC that influences the prognosis, staging and treatment decisions [2, 3]. The presence of LNM in CRC is a crucial factor that significantly influence local recurrence rates and patient survival outcomes [4, 5]. Studies indicated that the five-year overall survival rate of CRC patients without regional LNM is approximately 20% higher than that of patients with LNM [1, 6]. The National Comprehensive Cancer Network (NCCN) recommends preoperative neoadjuvant therapy for lymph node-positive patients, which significantly reduces the risk of local recurrence and enhances overall survival outcome [7]. Therefore, accurate assessment of lymphatic metastases before surgery is crucial for planning an effective and individual treatment strategy.

Computed tomography (CT) is the most widely employed diagnostic modality in staging CRC [8]. In evaluating lymph node status, CT primarily relies on morphologic characteristics such as size, shape, border contour, and enhancement patterns [9]. However, the reliability of CT in assessing lymph node involvement is limited due to the overlapping features of benign and malignant lymph nodes, which lack absolute specificity. For instance, the sensitivity of conventional CT diagnostic criteria based on lymph node size is only 50%-70%, which is insufficient to accurately identify all metastatic lymph nodes, especially small metastatic lymph nodes that are easily missed [10, 11].

Dual-energy CT (DECT) is an advanced imaging modality that provides multiple quantitative parameters of tissue characterization based on material decomposition. DECT shows significant promise in the assessment of lymph nodes by providing contrast and resolution and the ability to quantify parameters [12–15]. For instance, Yang et al. showed that normalized effective atomic number (Zeff) in the venous phase was the best DECT parameter for differentiating metastatic and non-metastatic lymph nodes, superior to morphologic criteria [16]. Dual layer spectral CT (DLSCT) is a detector-based DECT that simultaneously absorbs and differentiates high and low energy. This method ensures complete temporal and spatial coherence of spectral data, resulting in excellent data registration and image correspondence across different phases, and minimizes measurement errors [17]. Several studies demonstrated functional parameters derived from DLCT effectively evaluate metastatic lymph nodes in gastric cancer, lung cancer, and breast cancer [18–20]. However, the use of DLSCT in assessing LNM has not been extensively studied, and inconsistent findings regarding spectral parameters remains. Therefore, the aim of this study is to investigate the feasibility of quantitative parameters derived from DLSCT in assessing lymph node status in colorectal cancer.

Materials and methods

Participants

This retrospective study was approved by the institutional review board of our hospital (No.YE2024-342-01, approved on 29 September 2024) and was exempt from the requirement for informed consent due to its design. A total of 82 patients with pathologically confirmed CRC were consecutively collected from January 2022 to January 2024.

The inclusion criteria were: (1) the interval between preoperative DLSCT scans and curative surgery was two weeks; (2) pathological examination of lymph node specimens was conducted through a surgical procedure; (3) patients who did not receive preoperative radiotherapy or chemotherapy. The exclusion criteria were as follows: (1) emergency surgical cases; (2)patients with recurrent disease or prior colorectal resection; (3) regional lymph nodes on spectral images did not match postoperative pathology ($n = 5$); (4) poor image quality affected region of interest (ROI) outlining ($n = 8$); (5) tumors were not visible on DLSCT images ($n = 3$).The flowchart for patient selection is illustrated in Fig. 1.

DLSCT scan

An abdominal CT examination was performed using DLSCT (IQon Spectral CT, Philips Healthcare). The scan range extended from the top of the diaphragm down to 5 cm below the pubic symphysis. The triple-phase enhanced scan was conducted using a nonionic contrast agent with an iodine concentration of 370 mg/ml (Ultravist 370®, Bayer Healthcare, Berlin, Germany). Bolus tracking was performed by selecting an ROI within the abdominal aorta. The contrast agent was injected via an elbow vein at a dose of 1.2 ml per kilogram of body weight at a rate of 2.5 mL per second, followed by a 30 ml saline flush at the same rate. The acquisition of arterial phase (AP) was initiated once the Hounsfield units (HU) of ROI in the aorta reached the predetermined threshold of 150. Venous and equilibrium phase scans were obtained in the 40s and 90s following arterial phase. The acquisition parameters were set as follows: automated exposure modulation for tube current, 120 kVp tube voltage, 64×0.625 mm collimation, 0.4s rotation time, 1.1 spiral pitch, and image reconstruction layer thickness of 1.0 mm.

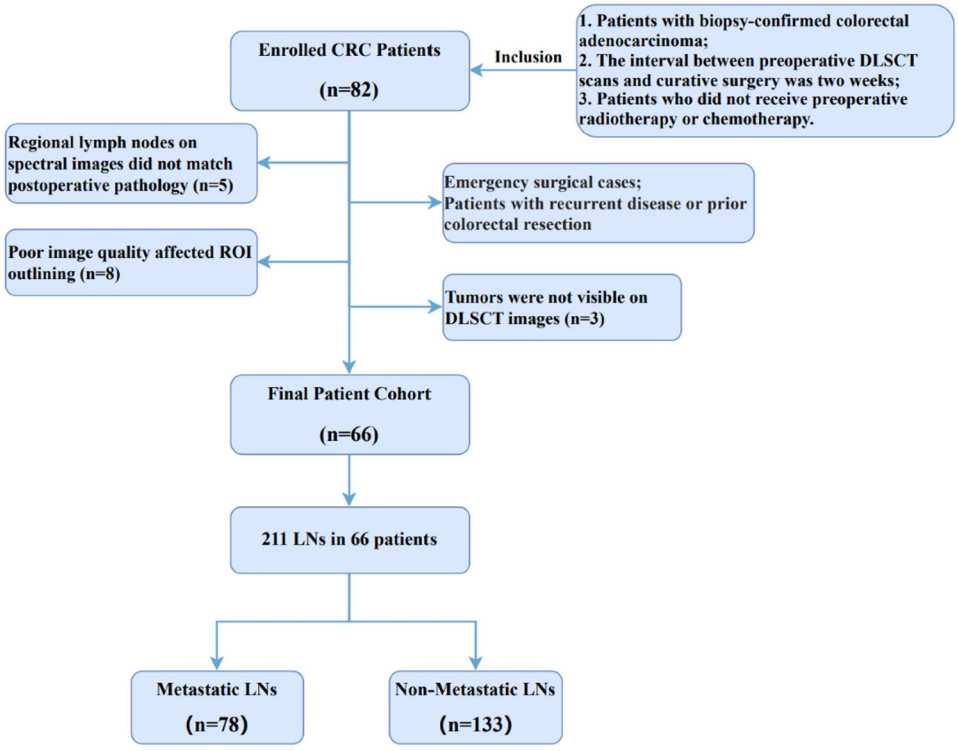

Fig. 1 Flow chart of patient recruitment in the study

Surgery and LN pathological-radiologic matching

All the patients in this study underwent surgery following standard colorectal surgical practice. Regional LNs were classified based on anatomical zones to enable a node-to-node comparison between radiological and pathological findings. Preoperative lymph node labeling was performed by a radiologist using 1 mm axial images with a 40-keV monochromatic arterial phase. The station numbers of LN were assessed based on the Japanese Classification of Colorectal, Appendiceal and Anal Carcinoma (JCCRC) [21]. The resection of colon cancer was performed to ensure clear lateral margins and included all the loco-regional lymph nodes associated with the resected bowel segment. The surgeon labeled the excised LNs based on their location in the CT image. In cases where all harvested LNs in a single CRC patient were either metastatic or non-metastatic, all identified LNs on the CT images were considered positive or negative for metastases, respectively. In cases involving both metastatic and non-metastatic LNs, we identified regional LNs from the pathological report based on the size and location (orientation, distance to rectal wall, or mesorectal fascia) of the LNs.

Morphological analysis of LNs on DLSCT

The morphological characteristics of each identified lymph node on DLSCT were evaluated and documented by two radiologists. These features included: (1) the maximum short diameter of the lymph nodes, measured using multiplanar reformation; (2) internal heterogeneity; and (3) ill-defined borders. Based on these CT morphological features, the radiologists independently determined the status of the lymph nodes.

DLSCT data analysis

All images were transferred to a Philips IntelliSpace Portal post-processing workstation and independently analyzed by two radiologists specialized in abdominal imaging with 6 years and 10 years of clinical experience, respectively, who were blinded to the pathological results. A freehand region of interest (ROI) was outlined around lymph nodes in both arterial and venous images to obtain DLSCT quantitative parameters, including the attenuation at 40Kev and 100Kev, iodine concentration (IC), and effective atomic number (Zeff) parameters. Areas of necrosis, vascularity, and calcification were intentionally avoided during this process. A circular ROI was drawn in the abdominal aorta or iliac artery at the same slice level of LNs to calculate normalized IC (NIC) and normalized Zeff (nZeff) to reduce individual variation. Furthermore, an ROI was delineated on the attenuation images at 40 keV and 100 keV of primary tumor to calculate the slope of the energy spectral curve (λHu). NIC, nZeff, λHu, and the ratio of the slopes of the lymph nodes to the slopes of the tumors (λHu-Ratio) were calculated using Eqs. (1), (2), (3), and (4), respectively.

$$NIC = IC_{LN} / IC_{vessel} \quad (1)$$

$$nZeff = Zeff_{(LN)} / Zeff_{(vessel)} \quad (2)$$

$$\lambda Hu = (CT_{40keV} - CT_{100keV}) / 60 \quad (3)$$

$$\lambda Hu - Ratio = \lambda Hu - LN / \lambda Hu - Tumor \quad (4)$$

Statistical analysis

Statistical analysis was conducted using GraphPad Prism v8, SPSS v27 and MedCalc 20.1.0 software. The intraclass correlation coefficient (ICC) was used to assess the interobserver assessment of DLSCT quantitative parameters. Quantitative parameters exhibiting a normal distribution were presented as mean ± standard deviation, whereas those without a normal distribution were presented as median (interquartile range). Group comparisons were conducted using the independent samples t-test or Mann-Whitney U test. For categorical variables, data are presented as frequencies (percentages). Group comparisons were performed using the Chi-square test. Fisher's exact test was applied under the following conditions to ensure validity: (1) when the total sample size (N) was < 40, or (2) when the expected frequency in any cell of the contingency table was < 1. The Spearman rank correlation coefficient was employed to assess the correlation of energy curve slopes between lymph nodes (LNs) and primary colorectal tumors. Univariate and multivariate binary logistic regression analyses were employed to identify parameters associated with LNM. The Hosmer evaluated the goodness-of-fit of the multivariate logistic model-Lemeshow test. The diagnostic efficacy of the multivariate model in determining lymph node status was assessed through receiver operating characteristic (ROC) curve analysis. DeLong's test was employed to compare the performance of the models. Decision curve analysis (DCA) was utilized to evaluate the clinical usefulness of the models by quantifying the net benefits for the treated. Statistical significance was defined as a P value of less than 0.05.

Results

Clinical characteristic

A total of 66 patients with colorectal adenocarcinoma who underwent colon surgery and regional lymph node resection were included in this study. D2 lymph node dissection, encompassing the paracolic and intermediate nodes, was conducted on patients with clinical T1 or T2 and N0 disease. For colon cancer in stages II and III, D3 lymph node dissection was performed to remove regional LNs which includes the paracolic, intermediate, and apical nodes. Eventually, 211 LNs were identified, including 133 non-metastatic LNs and 78 metastatic LNs. Among the 66 CRC patients, 24 were in the lymph node metastasis group, while 42 were in the non-lymph node metastasis group. No statistically significant differences were observed between the metastatic and non-metastatic lymph node groups for the majority of clinical-histological features, with the exception of pT staging ($P < 0.05$) and extramural venous invasion (EMVI) ($P < 0.001$). The detailed clinical characteristics of the patients was summarized in Table 1.

Morphologic analysis of LNs

The metastatic lymph nodes exhibited a notably larger maximum short-axis diameter compared to the non-metastatic lymph nodes (8.500mm[7.400–9.600] vs.7.400mm[6.300–8.500], $P < 0.001$). The internal heterogeneity and border were also different between metastatic LNs and non-metastatic LNs. All $P < 0.05$.

Quantitative DLSCT parameters analysis

The ICC values for the quantitative parameters assessed by two radiologists are provided [see Additional file 1], ranging from 0.925 to 0.989, indicating excellent reliability.

The quantitative parameters of metastatic and non-metastatic LNs are summarized in Table 2 and Fig. 2. In the arterial phase. Both the IC and NIC of metastatic LNs were significantly lower than those of non-metastatic LNs ($P < 0.001$). The Zeff and nZeff of metastatic LNs in the venous phase were significantly higher than those of non-metastatic LNs ($P < 0.001$). Additionally, the linear attenuation coefficient (λHu) of metastatic LNs was statistically higher than that of non-metastatic LNs in both the arterial and venous phases ($P < 0.001$). Although the IC and NIC values of metastatic lymph nodes in the venous phase were lower than those of non-metastatic lymph nodes, this difference is not statistically significant.

There was a positive correlation between λHu-LN and λHu-Tumor in the arterial and venous phases in the LN metastasis group, with Spearman correlation coefficients of 0.420 and 0.359, respectively (all $P < 0.001$). In the non-LN metastasis group, a weak correlation was observed between λHu-LN and λHu-Tumor, with a Spearman correlation coefficient of 0.253 ($P < 0.001$). However, no significant correlation was found in the arterial phase in this group. Figure 3 illustrates the correlation between λHu-LN and λHu-Tumor in the groups with LNM and those without lymphatic metastasis. Representative cases are shown in Figs. 4 and 5.

Univariate and multivariate logistic regression analysis

Univariate analysis of morphological features revealed that the maximum short axis, internal heterogeneity, and border characteristics were significantly associated with LNM, with P values of less than 0.001, 0.004, and 0.010, respectively. Furthermore, multivariate analysis

Table 1 Clinical and pathological characteristics of patients

Characteristics	All (*n* = 66)	LNM group (*n* = 24)	Non-LNM group (*n* = 42)	*P*-value
Age (y)				
≤ 50y	14 (21.2%)	2 (8.3%)	12 (28.6%)	0.053
>50y	52 (78.8%)	22 (91.7%)	30 (71.4%)	
Gender				
Female	25 (37.9%)	11 (45.8%)	14 (33.3%)	0.314
Male	41 (62.1%)	13 (54.2%)	28 (66.7%)	
EMVI				
Negative	28 (42.4%)	1 (4.2%)	27 (64.3%)	<0.001*
Positive	38 (57.6%)	23 (95.8%)	15 (35.7%)	
Tumor location				
Left colon	23 (34.8%)	9 (37.5%)	14 (33.3%)	0.944
Right colon	15 (22.7%)	6 (25.0%)	9 (21.4%)	
Rectum	25 (37.9%)	8 (33.3%)	17 (40.5%)	
Transverse colon	3 (4.5%)	1 (4.2%)	2 (4.8%)	
pT Stage				
T1	2 (3.0%)	0 (0.0%)	2 (4.8%)	0.033*
T2	3 (4.5%)	0 (0.0%)	3 (7.1%)	
T3	35 (53.0%)	10 (41.7%)	25 (59.5%)	
T4	26 (39.4%)	14 (58.3%)	12 (28.6%)	

Data are number of patients; data in parentheses are percentage unless otherwise indicated; significant results are shown by an asterisk (*$P < 0.05$). EMVI extramural venous invasion, pT pathological tumor stage. Percentages may not sum to exactly 100% due to rounding

Table 2 Morphological and quantitative DLSCT parameter of LNs

	Metastatic LNs (*n* = 78)	Non-Metastatic LNs (*n* = 133)	t/Z value	*P* value
Morphological Feature				
Short Axis Diameter(mm)	8.500 (7.400–9.600)	7.400 (6.300–8.500)	−4.206	< 0.001*
Internal Heterogeneity				
Yes	44 (56.4%)	101 (75.9%)	8.724	0.003*
No	34 (43.6%)	32(24.1%)		
Border				
Well-defined	46 (59.0%)	101(75.9%)	6.697	0.010*
Ill-defined	32 (41.0%)	32 (24.1%)		
DLSCT Parameter				
AP				
IC (mg/ml)	1.228 (0.870–1.601)	1.489(1.175–2.127)	−3.957	< 0.001*
NIC	0.117 (0.923 − 0.165)	0.168 (0.117–0.238)	−4.455	< 0.001*
Zeff	8.200 ± 0.304	8.081 ± 0.312	−4.975	< 0.001*
nZeff	0.746 (0.726–0.782)	0.742 (0.705–0.774)	−1.264	0.206
λHu-LN	2.057 (1.512–2.659)	1.590 (1.158–1.987)	−4.100	< 0.001*
λHu-Ratio	1.110 (0.910–1.625)	1.000 (0.745–1.285)	−3.258	< 0.001*
VP				
IC (mg/ml)	2.168 (1.544–2.846)	2.290 (1.788–2.825)	−0.827	0.408
NIC	0.368 (0.266–0.494)	0.417 (0.316–0.541)	−1.756	0.078
Zeff	8.699 (8.506–8.949)	8.280 (8.053–8.573)	−7.471	< 0.001*
nZeff	0.886 ± 0.377	0.860 ± 0.5170	−4.322	< 0.001*
λHu-LN	3.197 (2.764–3.840)	2.252 (1.647–2.953)	−7.457	< 0.001*
λHu-Ratio	1.360 (1.080–1.508)	0.960 (0.715–1.275)	−5.135	< 0.001*

Quantitative information that conforms to a normal distribution was expressed as Mean±Standard deviation. Non-normally distributed quantitative information was expressed as median percentage with the interquartile range in the parentheses. Qualitative information was depicted as the number of cases (percentage). Significant results are shown by an asterisk (*$P < 0.05$). AP arterial phase, VP venous phase, IC iodine concentration, NIC normalized iodine concentration, Zeff effective atomic number, nZeff normalized effective atomic number, λHu the slope of the spectral Hounsfield unit curve of lymph nodes, λHu-Ratio the ratio of slope of the spectral Hounsfield unit curve for lymph nodes to that for the spectral curve for tumors

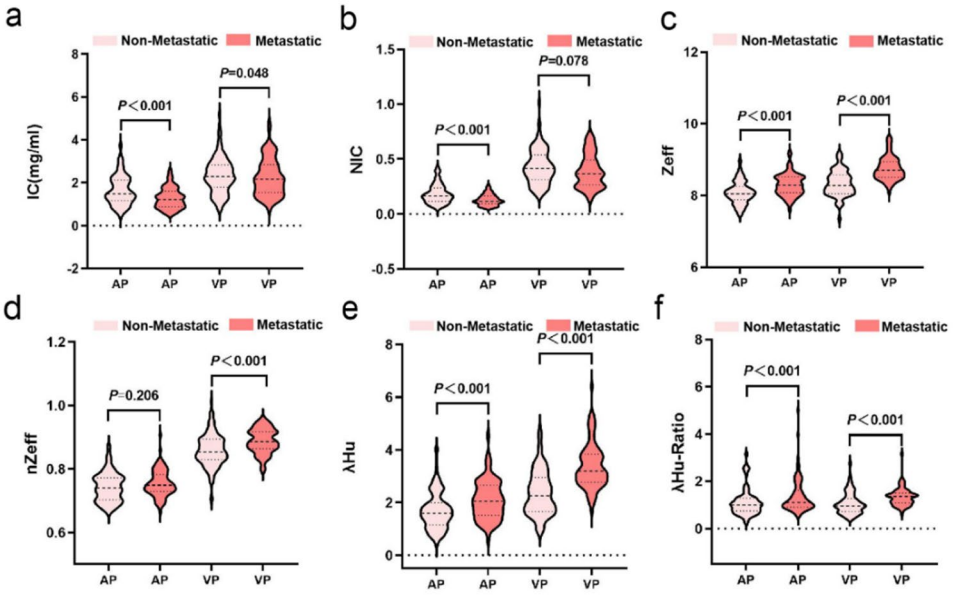

Fig. 2 Violin plots comparing DLSCT parameters in metastatic versus non-metastatic lymph nodes during the arterial and venous phases

of morphological features indicated that the maximum short axis serves as a predictive factor for LNM, with an OR of 1.317 (95% CI: 1.130–1.536, $P<0.001$).

Univariate logistic regression analysis of quantitative parameters obtained from DLSCT indicated that the following factors were significantly associated with LN metastasis in CRC patients: Zeff, λHu-LN, λHu-Ratio in both arterial phase and venous phases, IC, NIC in the arterial phase, nZeff in the venous phase (all $P<0.05$). In the multivariate analysis, IC (OR= 0.229, 95% CI: 0.076–0.689, $P=0.009$), NIC (OR= 0.000, 95% CI: 0.000-0.505, $P=0.033$) in the arterial phase and Zeff (OR= 4.012, 95% CI: 1.183–13.603, $P=0.026$), λHu-LN (OR= 3.237, 95% CI: 1.401–7.749, $P=0.006$) in the venous phase were identified as independent predictors for lymph node metastasis in CRC patients. Further details can be found in Table 3.

Diagnostic performance of morphological criteria and DLSCT parameters

The combined morphological features demonstrated an AUC of 0.695, with a sensitivity of 66.7% and specificity of 68.4%. In the univariate analysis of DLSCT parameters, the AUC for Zeff, λHu-LN, λHu-Ratio in both arterial phase and venous phases, IC, NIC in the arterial phase, nZeff in the venous phase ranged from 0.643 to 0.808. Among these parameters, both Zeff and λHu-LN in the venous phase yielded the highest AUC values (0.808 for both), with sensitivities of 89.7% and 87.2%, and specificities of 62.4% and 66.2%, respectively. The multivariate model incorporating DLSCT parameters demonstrated enhanced diagnostic performance, with an AUC of 0.901, 82.1% sensitivity, and 87.2% specificity, which was superior to other parameters as determined by the Delong test (Fig. 6). The DCA results indicated that the combined quantitative parameter model offered better net benefits for evaluating LNM than morphological features across entire reasonable threshold probability range (Fig. 7). Detailed data can be found in Tables 4 and 5.

Discussion

In this study, we assessed the efficacy of DLSC-derived parameters in differentiating LN status of patients with colorectal cancer. Our findings reveal that metastatic LNs exhibit lower IC and NIC, as well as higher Zeff, nZeff and λHu values compared to non-metastatic LNs. Furthermore, there is a notable positive correlation in λHu values between metastatic LNs and primary tumors in both arterial and venous phase. Multivariate analysis based on quantitative parameters achieved an AUC of 0.901 for predicting LN status, which surpassed that of morphological criteria.

We found that the IC and NIC of metastatic LNs were lower than those of non-metastatic LNs, especially in the arterial phase. This finding is consistent with previous studies [16, 22, 23]. IC quantifies the iodine concentration of tissue and indirectly indicates the blood supply. NIC reduces the individual variability and enhances the accuracy of iodine quantification. This result may be attributed to decreased blood flow in the metastatic LNs. Animal studies have demonstrated that perfusion defects, which can result from abnormal hemodynamics in neovascular vessels or a reduced blood flow, can arise within the parenchyma due to compression from LN tumor growth [24, 25]. These changes can occur

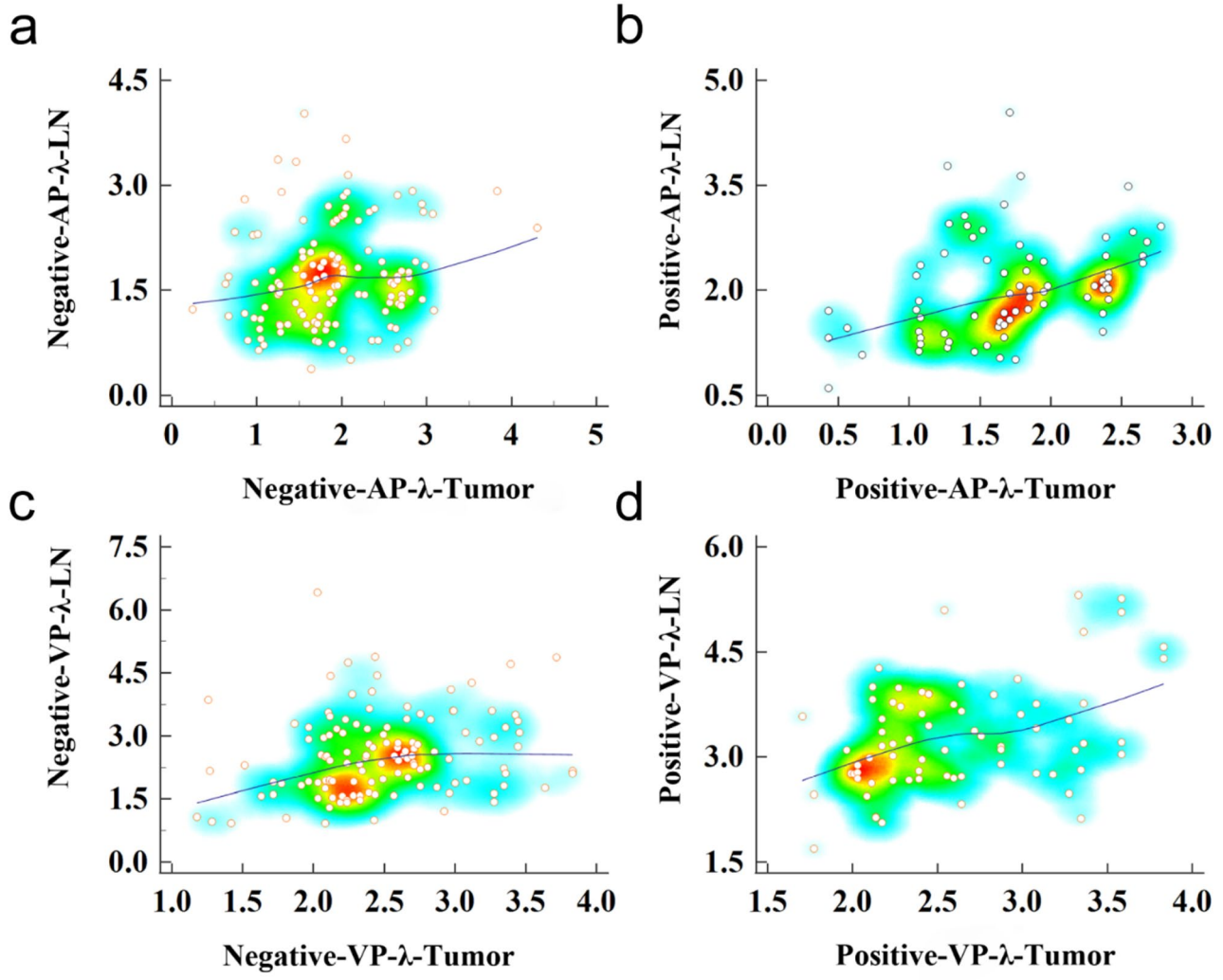

Fig. 3 Spearman rank correlation analysis of energy curve slopes between lymph nodes (LNs) and primary colorectal tumors. A positive correlation was observed between λHu-LN and λHu-Tumor in both the arterial and venous phases for the lymph node metastasis group, with Spearman correlation coefficients of 0.420 and 0.359, respectively (all $P < 0.001$). In contrast, the non-lymph node metastasis group exhibited a weaker correlation between λHu-LN and λHu-Tumor, with a Spearman correlation coefficient of 0.253 ($P < 0.001$)

even in the early stages of LN metastasis, particularly in non-enlarged nodes. A study by Jeong HS, et al. found that LNM exhibited a deficiency of vascular endothelial growth factor (VEGF-C, VEGF-D) and thrombospondin-1 (TSP-1) surrounding lymph node blood vessels, resulting in the lack of sprouting angiogenesis in LNM [26].

Furthermore, decreased lymphatic vessel density was observed in macrometastatic LNs, indicating that the presence of the cancer cells causes lymphatic vessel regression [26]. However, controversial findings regarding IC in LNM remained [16, 27]. We hypothesized this inconsistency may be attributed to biological variability, heterogeneity in lymph node involvement, and technical variability in DECT.

Zeff is a crucial functional parameter of dual energy CT that is related to the fundamental properties of elements. It characterizes structures in composite media based on material content and can enhance tissue differentiation [28]. The Zeff values of the metastatic and non-metastatic lymph nodes were significantly Different. Variations in material composition, such as hydrogen, carbon, and nitrogen, as well as significant changes in high-Z trace elements, occur during metastasis compared to healthy tissues [29]. Additionally, metastatic LNs exhibit increased iodine uptake and histopathological alteration. These factors collectively contribute to the higher Zeff values observed in metastatic LNs compared to non-metastatic ones. A prospective study by Yang et al. showed that the portal phase nZeff was the most effective DECT

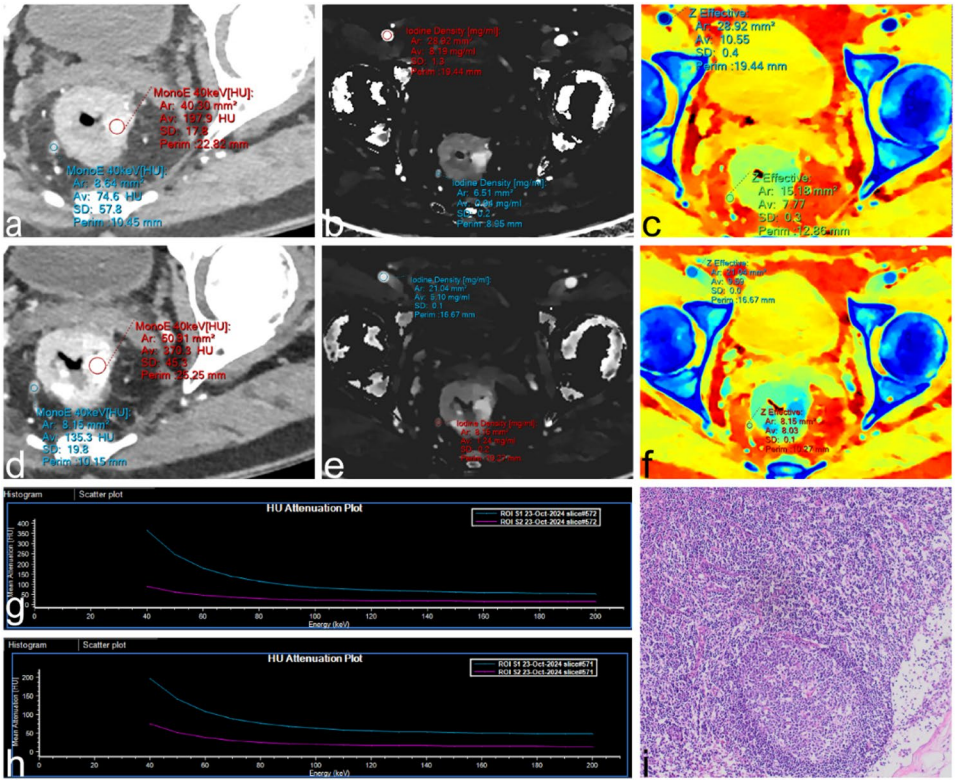

Fig. 4 A 41-year-old male patient with rectal cancer and non-metastatic LN is presented. The primary tumor (indicated by red circles) and the lymph node (indicated by blue circles) are depicted in 40-keV monochrome images during the arterial (**a**) and venous (**d**) phases. The mean iodine concentration of the lymph node is 0.94 mg/ml in the arterial phase (**b**) and 1.24 mg/ml in the venous phase (**e**). The mean effective atomic number of the lymph node is 7.77 in the arterial phase (**c** and 8.03 in the venous phase (**f**). The spectral energy curves of the primary tumor (blue curve) and the lymph node (purple curve) differ in both arterial (**g**) and venous (**h**) phases. Histological examination of the non-metastatic lymph node stained with hematoxylin and eosin (H&E) reveals the presence of germinal centers (×40) (**i**)

parameter for differentiating metastatic and non-metastatic LNs [16].

We observed higher λHu values in LNMs compared to non-metastatic LNs and a notable positive correlation in λHu values between metastatic LNs and primary tumors in both the arterial and venous phases. The λHu, which refers to the slope of the spectral Hounsfield unit curve characterizing attenuation changes across different energy levels, has been shown to be useful for differential diagnosis of lymph nodes. A similar study indicated a moderate correlation in λHu between primary breast cancer lesions and metastatic lymph nodes [30]. Analyzing the trend or slope correlation of the spectral curves helps evaluate the homology between different lesions. Lesions with different physiological properties display distinct trends in spectral curves. In contrast, lesions that are homologous or pathologically similar present comparable or coincident slopes in their spectral curves [31]. During the tumor-node metastasis process, tumor cells detached from the primary lesion and migrated directionally to the subperitoneal sinus region via input lymphatic vessels, where they proliferated and underwent angiogenesis to form metastatic foci at specific sites [32]. Therefore, the pathophysiological characterization and imaging manifestations of metastatic foci and metastatic lymph nodes are similar to those of primary lesions, resulting in a correlation between the slopes of the energy spectrum curves of both.

The morphological assessment is vital for diagnosing lymph node metastasis. We found that the maximum short-axis is a significant predictor of LNM in colorectal cancer, consistent with previous studies [33, 34]. However, relying solely on morphological criteria to assess LNM presents challenges, especially in assessing normal-size lymph nodes and identifying micrometastasis. The integration of quantitative DLSCT parameters into the multivariate model improved predictive performance and provided greater net benefits in evaluating lymph node status, achieving 82.1% sensitivity compared to 66.7% for morphologic criteria alone. This suggested that DLCST data can identify occult metastases in normal-sized nodes (< 10 mm) by detecting subtle changes in iodine distribution, Zeff and spectral slope, effectively overcoming the limitations of size-based staging and potentially reducing under-staging in clinical practice. Evaluating the clinical adoptability of DLCST requires its accuracy

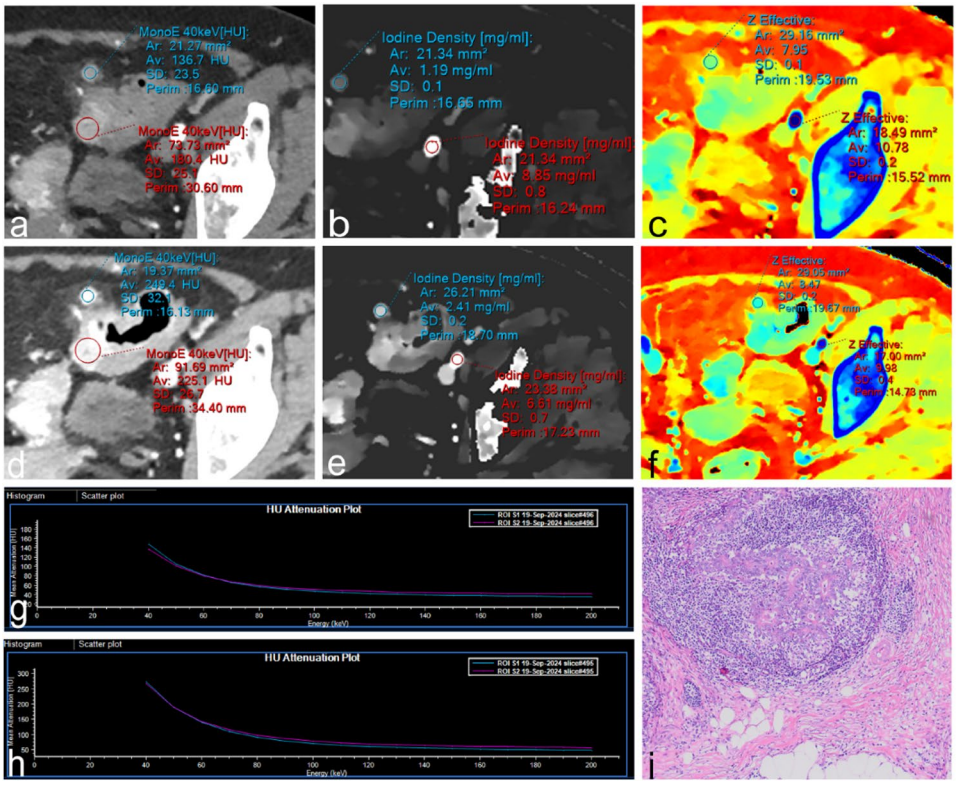

Fig. 5 A 65-year-old female patient with colon cancer and metastatic lymph node (LN). The primary tumor (indicated by red circles) and the metastatic lymph node (indicated by blue circles) are depicted in 40-keV monochrome images during the arterial (**a**) and venous (**d**) phases. The mean iodine concentration of the lymph node is 1.19 mg/ml in the arterial phase (**b**) and 2.41 mg/ml in the venous phase (**e**). The mean effective atomic number of the lymph node is 7.95 in the arterial phase (**c**) and 8.47 in the venous phase (**f**). The energy curves of the primary tumor (blue curve) and the metastatic lymph node (purple curve) overlap in both the arterial (**g**) and venous (**h**) phases. Histological examination of the metastatic lymph node stained with H&E confirms the presence of metastasis (×40) (**i**)

as well as practical factors such as radiation exposure and cost-effectiveness in routine radiological practice. DLSCT employs a single-source X-ray tube combined with dual-layer detectors and a retrospective acquisition scan mode. Studies demonstrated that DLSCT provides spectral information without increasing CT dose index (CTDI) or dose length product (DLP) compared to conventional single-energy protocols [35, 36]. Additionally, the availability of virtual non-enhanced images may enable omission of a true plain scan, thereby reduce the overall radiation dose to the patient. Moreover, the retrospective nature of DLSCT fundamentally enhances cost-effectiveness by ensuring that spectral data is inherently available for every acquisition, regardless of the initial clinical indication [37].

Our study has the following limitations. First, the single-center, retrospective design and limited sample size may introduce selection bias and restricted generalizability. Consequently, these findings require validation in larger, prospective, and multicenter studies. Second, lymph node metastasis patterns vary significantly with clinical stage and tumor localization; therefore, future research should prospectively stratify patients by colonic segment (e.g., right, left, rectum). Third, we only evaluated the conventional parameters of dual-energy CT (IC, Zeff, and λHu) using a manual ROI-like measurement approach. Previous studies demonstrated that DECT, when combined with radiomics or deep learning, may improve diagnosis accuracy, prognosis assessment, and prediction of treatment response across various cancer types [38–42]. Future studies should explore integrating DECT with radiomics or deep learning to stratify risk in CRC patients, including high-risk molecular or genetic biomarkers, and the prediction and assessment treatment response of neoadjuvant chemotherapy.

In conclusion, our findings indicate that the utilization of DLSCT-derived parameters provides significant value in differentiating lymph node metastasis in CRC patients by enabling the accurate assessment of tissue composition. By providing quantitative parameters that reliably distinguish metastatic from non-metastatic lymph nodes, DLSCT has the potential to identify high-risk patients who may benefit from preoperative systemic therapy. This strategy could support a significant shift in the therapeutic paradigm by enabling intensified treatment for

Table 3 Univariate and multivariate analysis of morphological features and quantitative DLSCT parameters predicting lymph node metastasis

	Univariate analysis		Multivariate analysis	
	OR (95% CI)	***P*-value**	**OR (95% CI)**	***P*-value**
Morphological Feature				
Maximum Short Axis	1.355 (1.167–1.573)	< 0.001*	1.317 (1.130–1.536)	< 0.001*
Internal Heterogeneity	0.410 (0.225–0.746)	0.004*	0.628 (0.216–1.828)	0.393
Border	0.455 (0.250–0.831)	0.010*	0.793 (0.272–2.312)	0.671
DLSCT Parameter				
AP				
IC (mg/ml)	0.326 (0.183–0.582)	< 0.001*	0.229 (0.076–0.689)	0.009*
NIC	0.331 (0.202–0.544)	< 0.001*	0.000 (0.000-0.505)	0.033*
Zeff	1.023 (1.013–1.033)	< 0.001*	1.021 (0.994–1.048)	0.134
nZeff	1.043 (0.978–1.111)	0.198	0.916 (0.799–1.048)	0.208
λHu-LN	2.184 (1.454–3.282)	< 0.001*	1.294 (0.433–3.867)	0.644
λHu-Ratio	1.983 (1.242–3.166)	0.004*	1.546 (0.744–3.213)	0.243
VP				
IC (mg/ml)	0.904 (0.646–1.267)	0.559	1.114 (0.521–2.384)	0.780
NIC	0.984 (0.965–1.002)	0.086	0.997 (0.995–1.042)	0.920
Zeff	10.833(5.386–21.789)	< 0.001*	4.012(1.183–13.603)	0.026*
nZeff	1.133 (1.061–1.209)	< 0.001*	0.972 (0.858–1.102)	0.659
λHu-LN	4.010 (2.608–6.168)	< 0.001*	3.237 (1.401–7.479)	0.006*
λHu-Ratio	4.216 (2.077–8.556)	< 0.001*	1.184 (0.295–4.750)	0.812

Significant results are shown by an asterisk (*$P < 0.05$). AP arterial phase, VP venous phase, IC iodine concentration, NIC normalized iodine concentration, Zeff effective atomic number, nZeff normalized effective atomic number, λHu the slope of the spectral Hounsfield unit curve of lymph nodes, λHu-Ratio the ratio of slope of the spectral Hounsfield unit curve for lymph nodes to that for the spectral curve for tumors

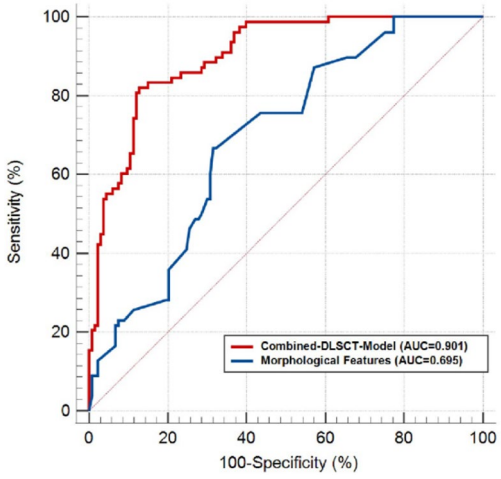

Fig. 6 ROC curve analysis demonstrates the diagnostic capability of the combined-DLSCT-model and morphological features for detecting lymph node metastasis

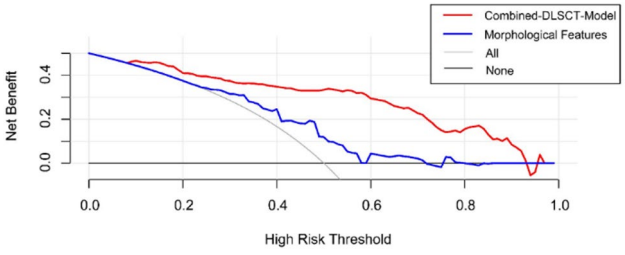

Fig. 7 The clinical utility of the combined-DLSCT-model and morphological features was assessed using a decision curve analysis (DCA) curve

node-positive cases and reducing neoadjuvant toxicity

Table 4 Diagnostic performance of morphological features in differentiating metastatic and non-metastatic LNs

Morphological Features	AUC (95% CI)	Sensitivity	Specificity	Accuracy	PPV	NPV	*P* value
Maximum Short Axis	0.673 (0.599–0.736)	73.1%	57.9%	63.5%	50.4%	78.6%	< 0.001*
Internal Heterogeneity	0.598 (0.528–0.664)	43.6%	76.2%	64.1%	51.7%	69.7%	0.004*
Border	0.585 (0.515–0.652)	41.0%	75.9%	63.0%	50.0%	68.7%	0.004*
Combined Model	0.695 (0.628–0.756)	66.7%	68.4%	67.8%	55.3%	77.8%	< 0.001*

Significant results are shown by an asterisk (*$P < 0.05$). AUC area under the curve, CI confidence interval, PPV positive predictive value, NPV negative predictive value

Table 5 Diagnostic performance of quantitative DLSCT parameters in differentiating metastatic and non-metastatic LNs

Parameters	AUC (95% CI)	Sensitivity	Specificity	Accuracy	PPV	NPV	*P* value
AP							
IC (mg/ml)	0.663 (0.589–0.727)	70.7%	57.1%	62.2%	49.2%	76.9%	< 0.001*
NIC	0.684 (0.614–0.748)	71.8%	57.9%	63.0%	50.0%	77.8%	< 0.001*
Zeff	0.697 (0.618–0.760)	61.5%	70.7%	67.3%	55.2%	75.8%	< 0.001*
nZeff	0.552 (0.473–0.622)	82.1%	35.3%	52.6%	42.7%	77.1%	0.193
λHu-LN	0.669 (0.592–0.734)	55.1%	75.2%	67.8%	56.6%	74.1%	< 0.001*
λRatio	0.643 (0.558-0.700)	89.7%	36.1%	55.9%	45.2%	85.7%	< 0.001*
VP							
IC (mg/ml)	0.534 (0.458–0.616)	38.5%	74.4%	61.1%	46.9%	67.4%	0.420
NIC	0.573 (0.494–0.652)	56.4%	61.7%	59.7%	46.3%	70.7%	0.080
Zeff	0.808 (0.744–0.857)	89.7%	62.4%	72.5%	58.3%	91.2%	< 0.001*
nZeff	0.672 (0.591–0.735)	78.2%	53.4%	62.6%	49.6%	80.7%	< 0.001*
λHu-LN	0.808 (0.741–0.854)	87.2%	66.2%	73.9%	60.2%	89.8%	< 0.001*
λHu-Ratio	0.712 (0.634–0.771)	78.2%	61.7%	67.8%	54.5%	82.8%	< 0.001*
Combined Model	0.901 (0.853–0.938)	82.1%	87.2%	85.3%	79.0%	89.2%	< 0.001*

Significant results are shown by an asterisk (*$P < 0.05$). AUC area under the curve, CI confidence interval, PPV positive predictive value, NPV negative predictive value, AP arterial phase, VP venous phase, IC iodine concentration, NIC normalized iodine concentration, Zeff effective atomic number, nZeff normalized effective atomic number, λHu the slope of the spectral Hounsfield unit curve of lymph nodes, λHu-Ratio the ratio of slope of the spectral Hounsfield unit curve for lymph nodes to that for the spectral curve for tumors

protocols in truly node-negative patients.

Abbreviations

AP	Arterial phase
AUC	Area under the curve
CI	Confidence interval
DCA	Decision curve analysis
DECT	Dual-energy CT
DLSCT	Dual layer spectrum CT
IC	Iodine concentration
ICC	Intraclass correlation coefficient
LNs	Lymph nodes
LNM	Lymph node metastasis
NIC	Normalized iodine concentration
nZeff	Normalized effective atomic number
NCCN	National Comprehensive Cancer Network
NPV	Negative predictive value
PPV	Positive predictive value
ROC	Receiver operating characteristic
ROI	Region of interest
VP	Venous phase
Zeff	Effective atomic number
λHu	Slope of the spectral attenuation curves
CTDI	CT dose index
DLP	Dose length product

Supplementary Information

The online version contains supplementary material available at https://doi.org/10.1186/s40644-026-01019-7.

Supplementary Material 1: Additional file 1. Consistency check results of two observers on each observation in the arterial and venous phases.

Acknowledgements
Not applicable.

Author contributions
LT: conceptualization, methodology, formal analysis, writing-original draft, data curation. GL: methodology, data curation, validation. XL: investigation, visualization. WC: funding acquisition, resources, Writing-Review & Editing. XL: supervision, project administration, resources, writing-review & editing. All authors reviewed the manuscript.

Funding
This work was supported by the Guangzhou Regional Clinical Characteristic Technology Project (Grant No. 2026P-TS060), Guangzhou Basic and Applied Basic Research Foundation (Grant No. 2023A03J0245), and National Nature Science of Foundation of China (Grant No.82202259).

Data availability
The data that support the findings of this study are available on request from the corresponding author. The data are not publicly available due to privacy or ethical restrictions.

Declarations

Ethics approval and consent to participate
This retrospective study was approved by Institutional Review Board of The Second Affiliated Hospital of Guangzhou University of Chinese Medicine (No. YE2024-342-01), waiving the need for written informed consent.

Consent to participate
This single-center, retrospective study was conducted in accordance with the Declaration of Helsinki and was approved by the Ethics Committee of The Second Affiliated Hospital of Guangzhou University of Chinese Medicine (No. YE2024-342-01). The requirement for written informed consent was waived by the aforementioned Ethics Committee due to the retrospective nature of the study.

Consent for publication
Not applicable.

Competing interests
The authors declare no competing interests.

Received: 24 September 2025 / Accepted: 11 March 2026
Published online: 21 March 2026

References

1. Siegel RL, Giaquinto AN, Jemal A. Cancer statistics, 2024. Cancer J Clin. 2024;74:12–49.

2. Kim HJ, Choi GS. Clinical implications of lymph node metastasis in colorectal cancer: current status and future perspectives. Annals coloproctology. 2019;35:109.
3. Jin M, Frankel WL. Lymph node metastasis in colorectal cancer. Surg Oncol Clin. 2018;27:401–12.
4. Chou JF, Row D, Gonen M, Liu YH, Schrag D, Weiser MR. Clinical and pathologic factors that predict lymph node yield from surgical specimens in colorectal cancer: a population-based study. Cancer: Interdisciplinary Int J Am Cancer Soc. 2010;116:2560–70.
5. Belderbos TD, van Erning FN, de Hingh IH, van Oijen MG, Lemmens VE, Siersema PD. Long-term recurrence-free survival after standard endoscopic resection versus surgical resection of submucosal invasive colorectal cancer: a population-based study. Clin Gastroenterol Hepatol. 2017;15:403–11. e401.
6. Jiang Y, Yuan H, Li Z, Ji X, Shen Q, Tuo J, et al. Global pattern and trends of colorectal cancer survival: a systematic review of population-based registration data. Cancer Biology Med. 2022;19:175–86.
7. Benson AB, Venook AP, Adam M, Chang G, Chen Y-J, Ciombor KK et, al. Colon cancer, version 3.2024, NCCN clinical practice guidelines in oncology. J Natl Compr Canc Netw 2024;22.
8. Nerad E, Lahaye MJ, Maas M, Nelemans P, Bakers FC, Beets GL, et al. Diagnostic accuracy of CT for local staging of colon cancer: a systematic review and meta-analysis. Am J Roentgenol. 2016;207:984–95.
9. Rollvén E, Blomqvist L, Öistämö E, Hjern F, Csanaky G, Abraham-Nordling M. Morphological predictors for lymph node metastases on computed tomography in colon cancer. Abdom Radiol. 2019;44:1712–21.
10. Miao S-S, Lu Y-F, Chen H-Y, Liu Q-M, Chen J-Y, Pan Y, et al. Contrast-enhanced CT imaging for the assessment of lymph node status in patients with colorectal cancer. Oncol Lett. 2020;19:3451–8.
11. Kawazoe T, Nakanishi R, Ando K, Zaitsu Y, Kudou K, Nakashima Y, et al. Preoperative CT lymph node size as a predictor of nodal metastasis in resectable Colon cancer: a retrospective study of 694 patients. BMC Gastroenterol. 2025;25:18.
12. Al-Najami I, Lahaye M, Beets-Tan RG, Baatrup G. Dual-energy CT can detect malignant lymph nodes in rectal cancer. Eur J Radiol. 2017;90:81–8.
13. Rizzo S, Radice D, Femia M, De Marco P, Origgi D, Preda L, et al. Metastatic and non-metastatic lymph nodes: quantification and different distribution of iodine uptake assessed by dual-energy CT. Eur Radiol. 2018;28:760–9.
14. Nagano H, Takumi K, Nakajo M, Fukukura Y, Kumagae Y, Jinguji M, et al. Dual-energy CT–derived electron density for diagnosing metastatic mediastinal lymph nodes in non–small cell lung cancer: comparison with conventional CT and FDG PET/CT findings. Am J Roentgenol. 2022;218:66–74.
15. Zhang X, Zheng C, Yang Z, Cheng Z, Deng H, Chen M, et al. Axillary sentinel lymph nodes in breast cancer: quantitative evaluation at dual-energy CT. Radiology. 2018;289:337–46.
16. Yang Z, Zhang X, Fang M, Li G, Duan X, Mao J, et al. Preoperative diagnosis of regional lymph node metastasis of colorectal cancer with quantitative parameters from dual-energy CT. Am J Roentgenol. 2019;213:W17–25.
17. Rassouli N, Etesami M, Dhanantwari A, Rajiah P. Detector-based spectral CT with a novel dual-layer technology: principles and applications. Insights into imaging. 2017;8:589–98.
18. Luo M, Chen G, Xie H, Zhang R, Yang P, Nie R, et al. Preoperative diagnosis of metastatic lymph nodes by CT-histopathologic matching analysis in gastric adenocarcinoma using dual-layer spectral detector CT. Eur Radiol. 2023;33:8948–56.
19. Gao L, Lu X, Wen Q, Hou Y. Added value of spectral parameters for the assessment of lymph node metastasis of lung cancer with dual-layer spectral detector computed tomography. Quant Imaging Med Surg. 2021;11:2622.
20. Buus TW, Sandahl M, Thorup KS, Rasmussen F, Redsted S, Christiansen P, et al. Breast cancer: comparison of quantitative dual-layer spectral CT and axillary ultrasonography for preoperative diagnosis of metastatic axillary lymph nodes. Eur Radiol Experimental. 2021;5:1–11.
21. Colon JSfCot R. Japanese classification of colorectal, appendiceal, and anal carcinoma: the 3d English edition [secondary publication]. J Anus Rectum Colon. 2019;3:175–95.
22. Liu H, Yan F, Pan Z, Lin X, Luo X, Shi C, et al. Evaluation of dual energy spectral CT in differentiating metastatic from non-metastatic lymph nodes in rectal cancer: Initial experience. Eur J Radiol. 2015;84:228–34.
23. Kato T, Uehara K, Ishigaki S, Nihashi T, Arimoto A, Nakamura H, et al. Clinical significance of dual-energy CT-derived iodine quantification in the diagnosis of metastatic LN in colorectal cancer. Eur J Surg Oncol (EJSO). 2015;41:1464–70.
24. Li L, Mori S, Kodama M, Sakamoto M, Takahashi S, Kodama T. Enhanced sonographic imaging to diagnose lymph node metastasis: importance of blood vessel volume and density. Cancer Res. 2013;73:2082–92.
25. Sakamoto M, Kojima I, Iikubo M, Ito K, Aoki T, Mori S, et al. Perfusion defects in non-enlarged metastatic lymph nodes using vessel wall magnetic resonance imaging: Detection performance and diagnostic value. Clin Exp Metastasis. 2022;39:421–31.
26. Jeong H-S, Jones D, Liao S, Wattson DA, Cui CH, Duda DG, et al. Investigation of the lack of angiogenesis in the formation of lymph node metastases. J Natl Cancer Inst. 2015;107:djv155.
27. Zou Y, Zheng M, Qi Z, Guo Y, Ji X, Huang L, et al. Dual-energy computed tomography could reliably differentiate metastatic from non-metastatic lymph nodes of less than 0.5 cm in patients with papillary thyroid carcinoma. Quant Imaging Med Surg. 2021;11:1354.
28. Agostini A, Borgheresi A, Mari A, Floridi C, Bruno F, Carotti M, et al. Dual-energy CT: theoretical principles and clinical applications. Radiol Med. 2019;124:1281–95.
29. Taylor M. Quantification of differences in the effective atomic numbers of healthy and cancerous tissues: a discussion in the context of diagnostics and dosimetry. Med Phys. 2012;39:5437–45.
30. Terada K, Kawashima H, Yoneda N, Toshima F, Hirata M, Kobayashi S, et al. Predicting axillary lymph node metastasis in breast cancer using the similarity of quantitative dual-energy CT parameters between the primary lesion and axillary lymph node. Japanese J Radiol. 2022;40:1272–81.
31. García-Figueiras R, Oleaga L, Broncano J, Tardáguila G, Fernández-Pérez G, Vañó E, et al. What to expect (and what not) from dual-energy ct imaging now and in the future? J Imaging. 2024;10:154.
32. Royston D, Jackson DG. Mechanisms of lymphatic metastasis in human colorectal adenocarcinoma. J Pathology: J Pathological Soc Great Br Irel. 2009;217:608–19.
33. Li S, Li Z, Wang L, Wu M, Chen X, He C, et al. CT morphological features for predicting the risk of lymph node metastasis in T1 colorectal cancer. Eur Radiol. 2023;33:6861–71.
34. Wang D, Zhuang Z, Wu S, Chen J, Fan X, Liu M, et al. A dual-energy CT radiomics of the regional largest short-axis lymph node can improve the prediction of lymph node metastasis in patients with rectal cancer. Front Oncol. 2022;12:846840.
35. Do TD, Rheinheimer S, Kauczor H-U, Stiller W, Weber T, Skornitzke S. Image quality evaluation of dual-layer spectral CT in comparison to single-layer CT in a reduced-dose setting. Eur Radiol. 2020;30:5709–19.
36. Picone C, Fusco R, Granata V, Porto A, Brunese MC, Zappia M, et al. Analysis of radiation dose reduction in oncological followup cases by using dual energy CT. Clin Translational Imaging. 2025:1–8.
37. Rajiah P, Rong R, Martinez-Rios C, Rassouli N, Landeras L. Benefit and clinical significance of retrospectively obtained spectral data with a novel detector-based spectral computed tomography-Initial experiences and results. Clin Imaging. 2018;49:65–72.
38. Lu H, Liu K, Zhao H, Wang Y, Shi B. Dual-layer detector spectral CT-based machine learning models in the differential diagnosis of solitary pulmonary nodules. Sci Rep. 2024;14:4565.
39. Wang T, Fan Z, Yue Y, Lu X, Deng X, Hou Y. Spectral dual-layer detector CT-based radiomics-deep learning for predicting pathological aggressiveness of stage I lung adenocarcinoma: discrimination of precursor glandular lesions and invasive adenocarcinomas. Translational Lung Cancer Res. 2025;14:431.
40. Li J, Dong D, Fang M, Wang R, Tian J, Li H, et al. Dual-energy CT–based deep learning radiomics can improve lymph node metastasis risk prediction for gastric cancer. Eur Radiol. 2020;30:2324–33.
41. Li M, Fan Y, You H, Li C, Luo M, Zhou J, et al. Dual-energy CT deep learning radiomics to predict macrotrabecular-massive hepatocellular carcinoma. Radiology. 2023;308:e230255.
42. Chen Y, Yuan F, Wang L, Li E, Xu Z, Wels M, et al. Evaluation of dual-energy CT derived radiomics signatures in predicting outcomes in patients with advanced gastric cancer after neoadjuvant chemotherapy. Eur J Surg Oncol. 2022;48:339–47.

Publisher's note